Static Load Test on Progressive Collapse Resistance of Precast Prestressed Hollow Core Slabs

Yun Zhou[1]; Baozheng Zhang[2]; Hyeon-Jong Hwang[3]; Jinnan Hu[4]; Kai Qian[5]; Zhengrong Zhu[6]; Weijian Yi[7]; Heng Pan[8]; and Su-Min Kang[9]

Abstract: Precast prestressed hollow core slabs (PPHCSs) are widely used in the construction of multistory cross-wall structures, but the floors are vulnerable to progressive collapse induced by unexpected loadings due to weak links between PPHCSs. Despite this fact, limited studies have been carried out on the progressive collapse resistance of PPHCSs. In this study, quasi-static tests were conducted to evaluate the progressive collapse resistance of PPHCSs. The test parameters were the types of connectors [i.e., single rebar connector (S1), double rebar connector (S2), partially debonded rebar connector (S3), kinked rebar connector (S4), and partial hinge rebar connector (S5)]. The progressive collapse resistance including the load-carrying capacity, deformation capacity, failure modes, and main load-resisting mechanism was evaluated. The energy dissipation capacity of all specimens was estimated based on the energy balance principle, and the energy dissipation capacity of S5 was 91%, 303%, 190%, and 85% greater than that of S1–S4, respectively. Further, the pseudo-static response of each specimen was calculated using a simplified dynamic assessment method. The test results revealed that all specimens generated effective compressive arch action and catenary action, and the ultimate strength (72.56 kN) of S5 using partial hinge was 64%, 334%, 110%, and 45% greater than that of S1–S4, respectively. **DOI: 10.1061/JSENDH.STENG-11902.**

Author keywords: Precast prestressed hollow core slab (PPHCS); Progressive collapse; Quasi-static test; Tie force; Catenary action; Simplified dynamic assessment.

Introduction

Precast prestressed hollow core slabs (PPHCSs), which possess the advantages of high strength, better quality control of materials, and high production efficiency, have been widely used in the construction of cross-wall structures for multistory residences and offices. The combination of prestressing force and low self-weight due to the voids of the slab section decreases the amount of reinforcement and concrete, without loss of structural performance. In the last few years, various studies on the shear behavior, flexural behavior, and thermal performance of PPHCSs have been performed (Cuenca and Serna 2013; Venanzi et al. 2014; Baran 2015; Mansour et al. 2015; Brunesi and Nascimbene 2015; Aguado et al. 2016; Kankeri and Prakash 2016, 2017; Michelini et al. 2020; Sarkis et al. 2022). However, the existing studies mainly focused on the behavior of individual PPHCS. The structural performance of PPHCSs in cross-wall structures, referring to the buildings using cross-walls as vertical load-bearing components and PPHCSs as floors, has rarely been evaluated. In comparison with conventional reinforced concrete (RC) structures, connections between PPHCSs in cross-wall structures can be identified as weak links due to the lack of continuity at the joint of PPHCSs. This implies that the floors are more sensitive to progressive collapse induced by unexpected loadings, such as gas explosions, vehicle impact, and uncontrolled fire, that exceed the allowable resistance of the structural system. Thus, sufficient continuity and ductility across the connection are necessary to provide tie force that can contribute to the development of an alternate load path.

Progressive collapse refers to the spread of an initial local failure from element to element, eventually resulting in the collapse of an entire structure or a disproportionately large part of it (ASCE 2005). Following the typical collapse including the Ronan Point apartment accident caused by a gas explosion in the United Kingdom in 1968 (Griffiths et al. 1968), the collapse of the Murrah Federal Building in Oklahoma City in 1995 (Corley et al. 1998), and the collapse of the World Trade Center in New York in 2001 (Seffen 2008), progressive collapse has attracted a lot of attention due to its disastrous safety consequences for people in buildings. Adam et al. (2018) presented an ambitious review of all the main advances that

[1]Professor, Key Laboratory for Damage Diagnosis of Engineering Structures of Hunan Province, Hunan Univ., Changsha 410082, China; Professor, College of Civil Engineering, Hunan Univ., Changsha 410082, China; Professor, Key Laboratory of Building Safety and Energy Efficiency of the Ministry of Education, Hunan Univ., Changsha 410082, China. Email: zhouyun05@hnu.edu.cn

[2]Postgraduate Student, College of Civil Engineering, Hunan Univ., Changsha 410082, China (corresponding author). Email: zhangbz@hnu.edu.cn

[3]Associate Professor, School of Architecture, Konkuk Univ., Seoul 05029, Korea. ORCID: https://orcid.org/0000-0002-7757-7540. Email: hwanggun85@naver.com

[4]Postgraduate Student, College of Civil Engineering, Hunan Univ., Changsha 410082, China. Email: hu1110@hnu.edu.cn

[5]Professor, College of Civil Engineering and Architecture, Guilin Univ. of Technology, Guilin 541004, China. Email: qiankai@glut.edu.cn; qian0024@ntu.edu.sg; qiankai@ntu.edu.sg

[6]Senior Engineer, College of Civil Engineering, Hunan Univ., Changsha 410082, China. Email: zhengrongzhu@hnu.edu.cn

[7]Professor, College of Civil Engineering, Hunan Univ., Changsha 410082, China. Email: wjyi@hnu.edu.cn

[8]Engineer, China Construction Third Bureau First Engineering Co., Ltd., 768 Gaoxin Ave., Hongshan District, Wuhan 430040, China. Email: 40198374@qq.com

[9]Associate Professor, School of Architecture, Soongsil Univ., Seoul 08826, Korea. Email: kangsm@ssu.ac.kr

Note. This manuscript was submitted on July 28, 2022; approved on May 15, 2023; published online on July 3, 2023. Discussion period open until December 3, 2023; separate discussions must be submitted for individual papers. This paper is part of the ***Journal of Structural Engineering***, © ASCE, ISSN 0733-9445.

had occurred since the beginning of the 21st century in the field of progressive collapse and robustness of buildings. Yi et al. (2021) quantitatively revealed prevailing experimental assumptions and configurations among over 100 series experiments for the progressive collapse behavior of RC frame structures. Alshaikh et al. (2020, 2022) systematically summarized previous experimental studies on the progressive collapse of various types of RC structures and conducted a comprehensive review of the most significant advancements in terms of enhancing the progressive collapse resistance of precast concrete structures. In addition, many researchers have focused on resistance mechanisms and methods to prevent the progressive collapse of building structures during accidents. For example, the alternative load path approach (Stinger and Orton 2013) has become one of the most widely used approaches to investigate the progressive collapse resistance of a structure. Under a column removal scenario, compressive arch action (CAA) and catenary action (CTA) can be generated (Elsanadedy et al. 2017), which are the main resistance mechanisms against progressive collapse. Yi et al. (2008) demonstrated the feasibility of using a static unloading approach to simulate column loss and reported that the predicted resistance of a typical RC frame based on the plastic limit state was approximately 70% of the tested failure capacity including CTA. Ravasini et al. (2021) used nonlinear dynamic finite element analysis to investigate the progressive collapse resistance of a precast concrete (PC) frame building. Kakhki et al. (2022) evaluated the progressive collapse of RC frames addressing soil-structure interaction.

In order to mitigate progressive collapse risk, various solutions were proposed. Yu and Tan (2014) tested RC frame specimens with special detailing techniques, including the use of an additional reinforcement layer at the midheight of the beam section, partially debonding bottom bars in the joint region, and partial hinges at one beam depth away from the column face. Feng et al. (2017) and Qiang et al. (2020) proposed a novel kinked rebar configuration to enhance both the seismic and progressive collapse resistances of RC frames, improving the load-carrying capacity and deformation capacity under the catenary mechanism of RC substructures. Alogla et al. (2016) provided additional bars at the midlayer of the RC beam section to mitigate progressive collapse and reported that the proposed scheme significantly improved the ductility and collapse resistance of RC beams subject to a column removal scenario. In general, CTA can be significantly weakened due to strain concentration and premature fracture of longitudinal bars. Addressing such a problem, Yang et al. (2021) proposed a novel method by embedding partially debonded rebars at the midheight of the beam section in the plastic hinge region. Compared to conventional substructures, the debonded rebars significantly increased the progressive collapse resistance of RC substructures. To consider the effect of slab on the progressive collapse resistance, Qian and Li (2018, 2013) investigated the performance of PC beam-slab substructures and RC flat slab specimens with/without strengthening externally bonded CFRP laminates. The test results demonstrated that the welded connection decreased the progressive collapse resistance of the PC specimen showing brittle failure, while the pinned connection developed considerable tensile membrane action. The strengthening schemes effectively improved the progressive collapse resistance of RC flat slabs.

However, the existing studies have mainly focused on beam-column substructures with/without slabs, whereas little attention has been paid to the progressive collapse resistance of PPHCSs. Tohidi et al. (2014), Tohidi and Baniotopoulos (2017), and Tohidi and Janby (2020) investigated the CTA of PPHCS structures under the removal of intermediate wall supports and reported that the specimens showing rebar fracture collapsed prior to the development of CTA, but the specimens showing pull-out failure exhibited clear evidence of CTA, which was consistent with the study of PCA (1975). Although the existing test results revealed that the CTA could be effectively triggered by the bar-slip and large deflection, the peak strength of CTA did not exceed that of CAA much. This result implies that the improvement of progressive collapse resistance provided by CTA is limited. Further, the existing tests did not consider the constraint of the upper walls on both sides of the hollow core slab, which somewhat differed from the actual situation. Thus, to ensure that a whole structure can resist the progressive collapse after the failure of vertical supporting walls, it is of great importance to design simple and cost-effective connections between PPHCSs.

In the present study, to investigate the progressive collapse resistance of PPHCSs, quasi-static tests were performed on five PPHCS-wall substructures. Five types of connectors (i.e., single rebar connector, double rebar connector, partially debonded rebar connector, kinked rebar connector, and partial hinge rebar connector) were adopted for PPHCS connections. The load-carrying capacity, ultimate displacement, failure modes, load-resisting mechanism, strain development of connectors, and energy dissipation capacity were evaluated. Further, the pseudo-static response of each specimen was estimated using a simplified dynamic assessment to evaluate the progressive collapse resistance of the specimens. On the basis of the results, the structural characteristics of each connection detail were discussed.

Test Program

Design of Test Specimens

A conventional multistory PC cross-wall structure using PPHCSs is shown in Fig. 1. This kind of structure has been mainly used as a residential building in rural areas of China, and only the gravity and

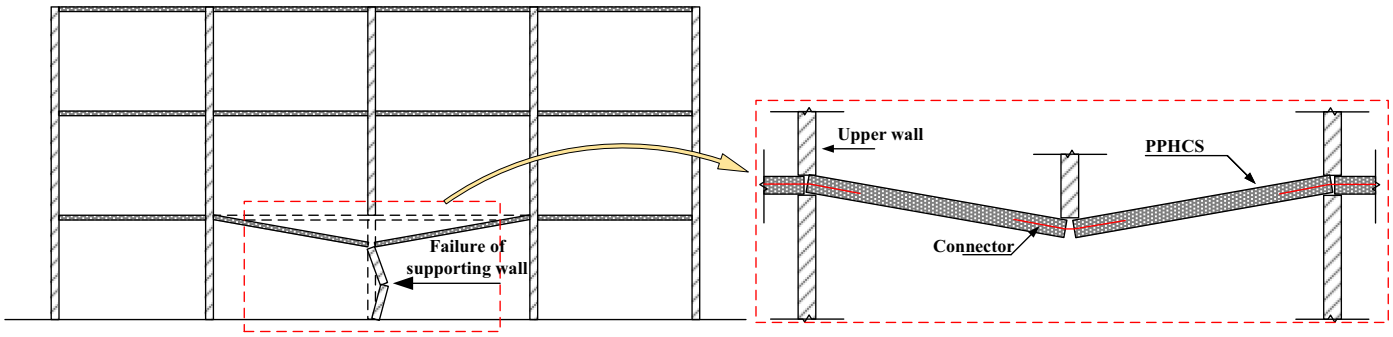

Fig. 1. Extraction of the test specimen.

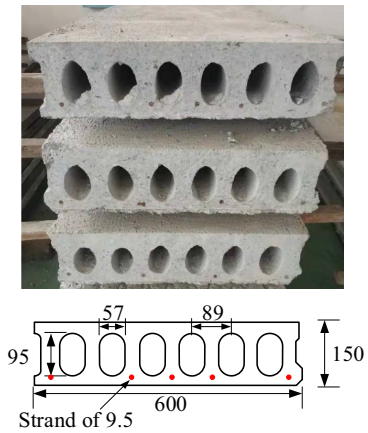

Fig. 2. Precast prestressed hollow core slab (PPHCS) (unit: mm).

wind loads are considered in the design process. Gravity load is sustained by one-way PPHCS simply supported on vertical supporting wall panels. The gap between PPHCSs is filled with mortar and has deficient continuity, which cannot provide sufficient resistance under accidental load compared with conventional RC structures. Under the failure of the supporting wall, the assembly between two PPHCSs is the most critical area, which requires sufficient strength and ductility to develop an effective alternative load path against progressive collapse. In this study, a wall-PPHCS substructure after the failure of a supporting wall is considered a test specimen, which consists of a pair of PPHCSs at two spans in the longitudinal direction and the survived wall panels.

In general, 1,200 mm wide hollow core slabs are manufactured, but tests using normal-size PPHCS can hardly be conducted due to the limited condition for test setup. Considering the width of PPHCS is not crucial since it is regarded as a kind of one-way slab, the PPHCS with a dimension of $2{,}700 \times 600 \times 150$ mm (cut through the middle) is used in this study (Fig. 2). Zero slump fine aggregate concrete with compressive strength of 40 MPa was used, and 1,209 kN of prestressing force was applied using five 9.5 mm strands with the tensile strength of 1,860 MPa (i.e., 65% of prestressing). Due to the hollow core structure, the self-weight of the slab is merely 2.5 kN/m^2.

The proposed connectors (C1–C5) were used in five specimens (S1–S5), respectively (Fig. 3). To develop CTA in cross-wall-PPHCS substructures, five types of connectors (C1–C5) for PPHCSs were designed based on the tie method [Fig. 3(b)]. In each specimen, four connectors were used. For sufficient anchorage of connectors, the embedment length of the connectors according to GB 50010-2010 (SAC 2010) was moderately amplified to 350 mm. Considering the tolerance of installation and the needs for grouting, a 50 mm gap was preserved in the middle joint between PPHCSs. High-strength grouting material was used to ensure reliable bond strength between the connectors and PPHCSs.

Connector C1 adopted a single straight T12 bar [i.e., diameter $(d_b) = 12$ mm and cross-sectional area $(A_s) = 113.04$ mm^2] at the center of the PC slab hole (i.e., tensile strength ratio of the total connector to slab section = 27.5%). Connector C2 comprised double straight T8 bar (i.e., $d_b = 8$ mm and $A_s = 50.24$ mm^2) at the upper and lower of the precast slab holes (i.e., tensile strength ratio of the total connector to slab section = 24.4%). To facilitate the fabrication and installation, rectangular shape of rebars were used in C2. Connectors C3, C4, and C5 were designed based on C2 (i.e., rectangular shape), and different special details were adopted. For C3, a 500 mm long local debonding area was introduced in the middle of the connector by wrapping PVC tubes, which was expected to increase the ultimate rotation capacity for sufficient development of CTA (Yang et al. 2021). In C4, a kinked rebar configuration was used, and soft foam that could be easily damaged during the straightening process was placed under the kinked area. Due to the large deformability of kinked rebar, CTA can be enhanced (Qiang et al. 2020). In C5, a partial hinge was placed in the middle of the connector, which was expected to improve the ultimate rotation capacity and enhance CTA (Yu and Tan 2014).

Specimen assembly (construction) steps are as follows: First, small holes are drilled on only the hollow cores inserting connectors at 575 mm away from the edge of the slab. Second, foam is inserted into the hollow core as a plug (refer to Fig. 3). For installation of a connector at each hollow core, plugs are installed at 600 mm (left side of the middle joint) and 1,200 mm (right side of the middle joint) away from the edge of the slab, which can accommodate the entire connector. At the other hollow cores without connectors, plugs are installed at the edge of the slab to avoid grout infiltration. Third, connectors are inserted into the hollow core. At the middle joint, the connectors are inserted into the right slab temporarily. At the edge joints, the connectors are installed directly. Fourth, two PPHCSs are assembled. Fifth, the connectors at the middle joint are centered through the 50 mm wide gap. Sixth, after the formwork is installed, grout is poured through the 50 mm wide gap until the grouting material flows out of the small holes.

Material Properties

In order to obtain the strength properties of the material used in test specimens, material tests were conducted. Three standard cubes of $100 \times 100 \times 100$ mm for concrete and three standard cubes of $70.7 \times 70.7 \times 70.7$ mm for grouting were cast and cured under the same condition as the test specimens. Material tests were conducted synchronously with the test of the specimens. The average compressive strength of three cubes was 52.5 MPa for concrete and 70.3 MPa for grout. Three sample coupons for each type of steel reinforcement were tested under uniaxial tension by an electrohydraulic servo testing machine to determine the yield strength and ultimate strength, and the elongation was measured by a clip extensometer. The mean value of the test results is presented in Table 1.

Test Setup and Instrumentation

The test setup and instrumentation were designed to simulate the scenario in which an underlying support wall fails [Fig. 4(a)]. Fig. 4(c) shows the boundary condition of the specimen, which is between fixed and pin boundary conditions. The specimen was horizontally restrained by a slotted steel beam, which was connected with the reaction frame by two screw bolts, and the stiffness of horizontal restraint was around 18 kN/mm according to the regression analysis of the relationship between horizontal reaction force and lateral displacement. Two 30 t load cells were installed in the middle of the screw bolts to measure the horizontal reaction force. The connector protruding from the PPHCS end passed through the slots, which were anchored to the slotted steel beam [Fig. 4(d)]. It is noted that the outward and inward movement of the slab ends is restrained by the slotted beam and bolt connection at the slotted beam, respectively, describing continuous slabs in multispans. To consider the weight of the upper walls at the ends of the PPHCS specimen, vertical restraint was provided by steel beams, which were anchored to the strong floor by anchor bolts. A steel pier was used to consider the lower vertical supporting wall. To measure the initial vertical load, strain gauges were attached to the anchor bolts. An initial vertical load of 11 kN was applied to

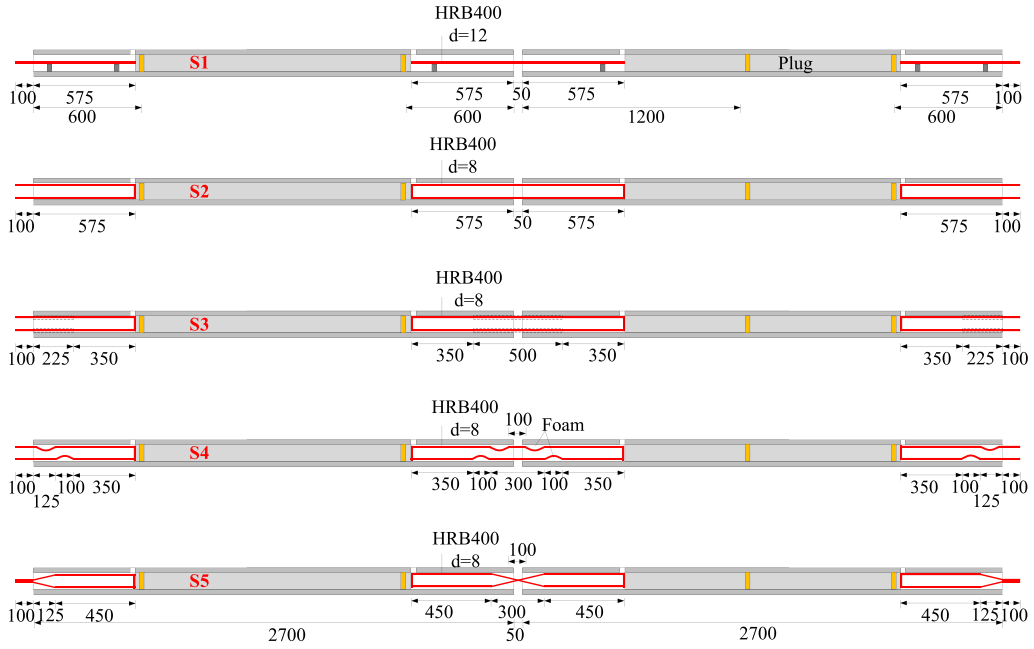

(a)

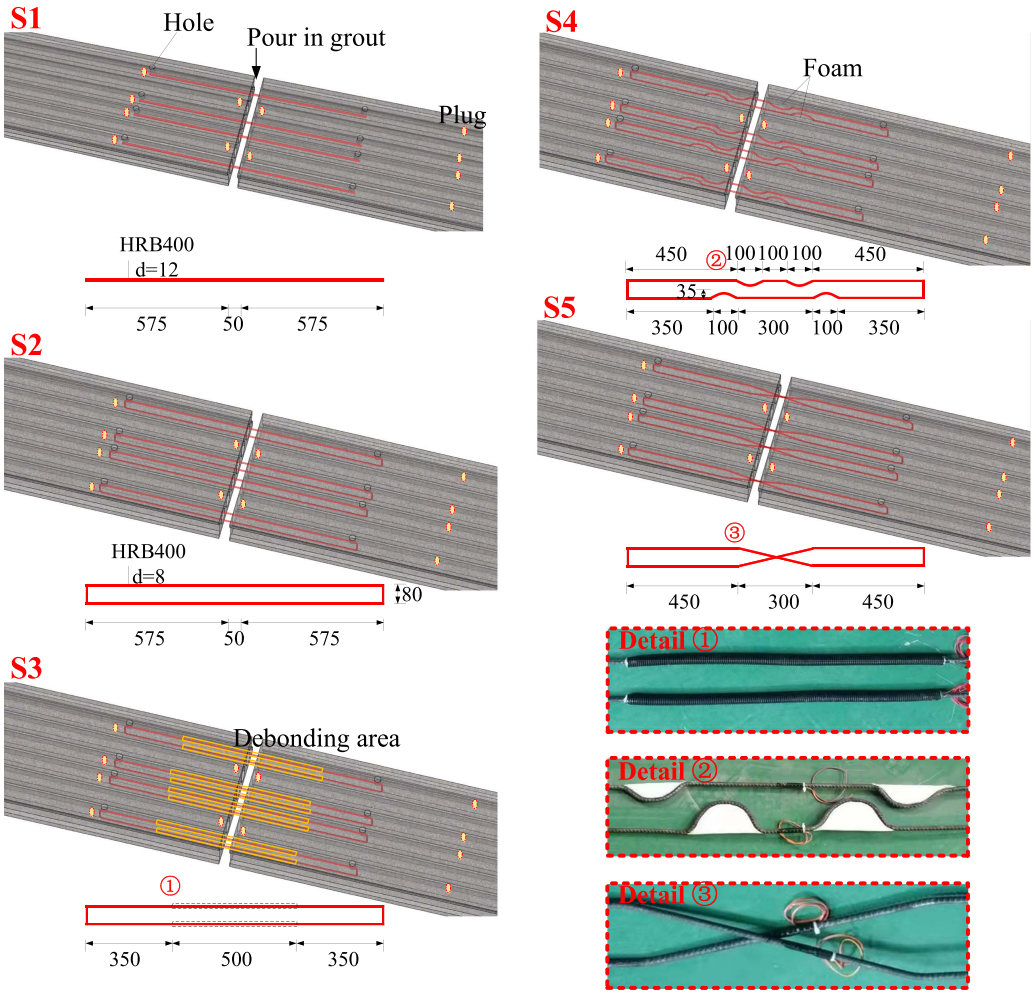

(b)

Fig. 3. Specimen configuration (unit: mm): (a) cross section; and (b) joint details.

Table 1. Material properties of steel reinforcements

Types	Nominal diameter (mm)	Yield strength f_y (MPa)	Ultimate strength f_u (MPa)	Elongation (%)
T8 (HRB400)	8	439.1	625.3	21.8
T12 (HRB400)	12	434.3	626.4	24.3
Strand	9.5	—	1,931.2	—

Note: Value of characteristic 0.1% proof-stress $f_{p0.1k}$ of the strand is 1,600 MPa.

each steel beam before loading to apply the weight of two-story brick walls on the slab ends. Since only half of the width of the upper wall (i.e., thickness of 250 mm) was mounted on the slab, a steel plate with a width of 100 mm was placed between the steel beam and specimen to consider the actual situation. It is noted that by addressing the symmetric test setup, the horizontal reaction force was measured only on the left side.

The details of the loading device are illustrated in Fig. 4(b). A vertical load was applied by a hydraulic jack on the top of the middle joint, and another jack was installed at the bottom of the middle joint for unloading. A 10 t load cell was laid on the top of a steel plate that was bolted on the reaction beam. With the elongation of the jack, the load cell was raised along with the steel plate and came into contact with the reaction beam, at which point the load cell began to measure the vertical load. To prevent the deformation of the jack under a large deflection of PPHCS specimens, a spherical hinge was set beneath the jack, allowing a slight rotation of the jack. The vertical load was distributed to both PPHCSs by a distribution beam. A roller welded on a steel plate was used to allow the relative rotation between the support and distribution beam and to restrict the displacement between the support and specimen. A lower hydraulic jack with a load cell (LC2) was installed to resist the beam self-weight (i.e., simulation of a supporting wall) at first. During the test, the lower hydraulic jack was gradually retracted to simulate the supporting wall failure, and the dead load due to the self-weight of the specimen and upper hydraulic jack was measured from LC2. A quasi-static loading was then applied using the upper hydraulic jack until the specimen failed, and the load was measured by the upper load cell (LC1). To obtain a reasonable load-displacement curve, a hybrid loading procedure was adopted. The force-controlled loading mechanism was employed at the initial stage of the test (i.e., 0.5 kN increment at each step). After the peak load of CAA, the displacement-controlled loading with the increment of 10 mm at a rate of approximately 0.2 mm/s at each step was conducted.

In practice, when a supporting wall is collapsed, the slab would be subjected to the impact load generated from the upper wall (Tohidi and Baniotopoulos 2017). The resulting structural damage and load path transfer usually occur in a very short time, revealing the nature of a dynamic effect. Although the dynamic effect was not considered in this test, the failure process and mechanism of specimens under quasi-static load were studied, and the dynamic effect was theoretically analyzed in the section "Simplified Dynamic Assessment."

In order to monitor the development of displacement and internal stresses for different phases, LVDTs and strain gauges were installed (Fig. 5). The vertical displacements of the PPHCS specimens were measured by six linear variable differential transformers (LVDTs) at the location from VD1 to VD6. Two dial indicators were used to measure the lateral displacements at the end of the specimen (i.e., LD1 and LD2). To measure strain increments, many strain gauges were attached to the connectors.

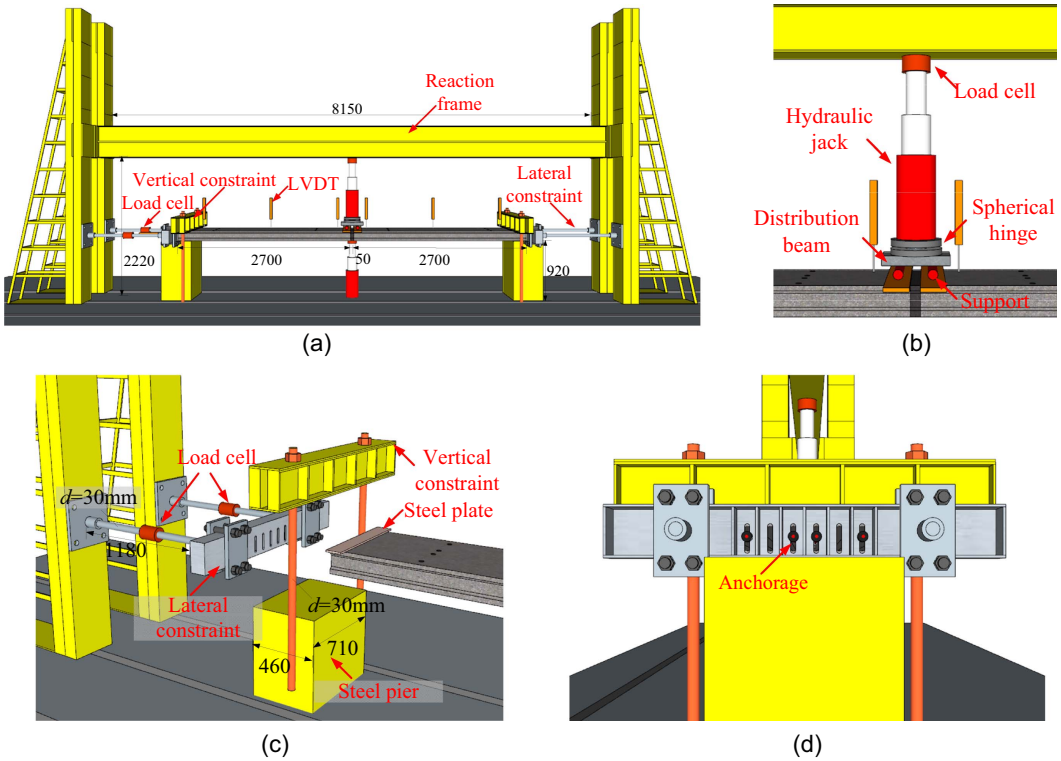

Fig. 4. Test setup and boundary condition (unit: mm): (a) overall test setup and instrumentation; (b) details of middle joint; (c) boundary condition of left joint; and (d) anchorage at slotted beam.

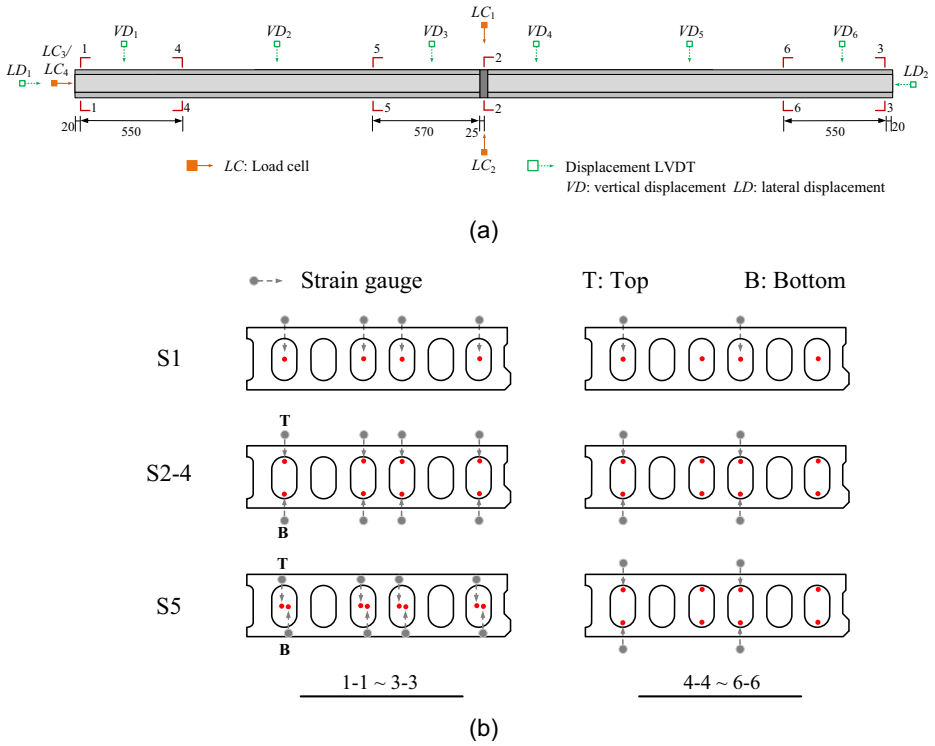

Fig. 5. Measurement instrumentation (unit: mm): (a) displacement; and (b) strain of connectors.

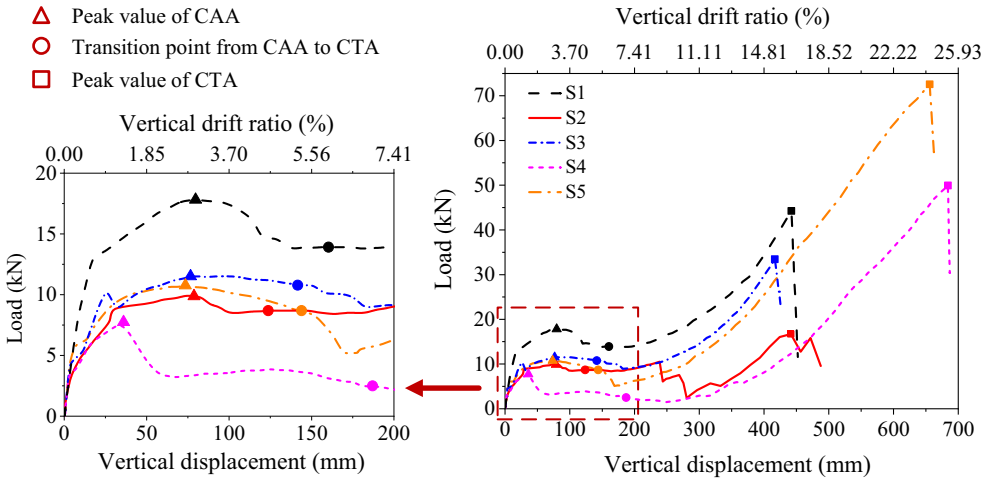

Fig. 6. Vertical load-displacement relationships of test specimens.

Test Results

Load and Reaction Force-Displacement Relationships

The vertical load-displacement relationships at the midjoint of the PPHCS specimens are presented in Fig. 6. The vertical drift ratio defined as the ratio of the downward displacement to the span length is also presented. Table 2 summarizes the test results. The load resistance mechanism can be divided into two main stages (i.e., CAA and CTA), and the peak load in CTA was greater than that of CAA. This result indicates that effective ties are generated at the slab joints. Fig. 7 shows the horizontal reaction force-vertical displacement relationships of the PPHCS specimens. In CAA, the horizontal reaction force was negative (i.e., compression force). As the vertical displacement increased, the horizontal reaction force was transferred to positive (i.e., tension force), indicating the beginning of CTA.

In specimen S1, flexural cracks first appeared at the interface between the slab end and grout when the vertical displacement (δ) reached 4.4 mm, but structural stiffness was not significantly decreased due to the effective lateral constraints of the edge joints. The peak load (P_{CAA}) in CAA was 17.81 kN at $\delta = 79.7$ mm, and the corresponding horizontal reaction force (R_H) reached the peak value in compression. After the peak load, the load-carrying capacity decreased gradually, and CTA occurred at $\delta = 160.3$ mm. Due to the tensile force generated in the connectors, the peak load (P_{CTA})

Table 2. Test results

Specimen	CAA			Transition point		CTA			$\frac{P_{CTA}}{P_{CAA}}$ (%)
	P_{CAA} (kN)	δ (mm)	δ/l (%)	δ (mm)	δ/l (%)	P_{CTA} (kN)	δ (mm)	δ/l (%)	
S1	17.81	79.7	3.0	160.3	5.9	44.24	442.2	16.4	248
S2	9.87	78.7	2.9	123.7	4.6	16.72	441.5	16.4	169
S3	11.51	76.6	2.8	141.6	5.2	34.55	416.8	15.4	300
S4	7.74	36	1.3	187	6.9	49.95	684.1	25.3	645
S5	10.76	73.5	2.7	143.9	5.3	72.56	655.9	24.3	674

Note: P_{CAA} and P_{CTA} denotes the peak strength of CAA and CTA, respectively; δ denotes the vertical displacement; l denotes the length of a PPHCS, which is 2,700 mm; and transition point denotes the point where CAA is converted to CTA.

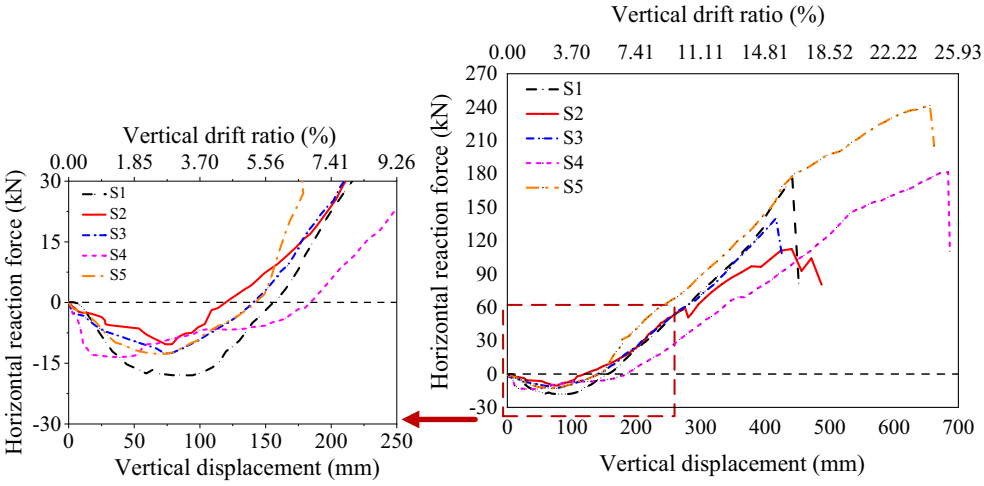

Fig. 7. Horizontal reaction force-vertical displacement relationships of test specimens.

in CTA increased to 44.24 kN at $\delta = 442.2$ mm. The corresponding R_H reached the peak value in tension. Ultimately, the test was terminated by the sudden crack at about 600 mm away from the slab edge under a negative moment. In general, the development of CTA requires relatively large vertical displacement. The vertical displacement-to-span ratio is $\delta/l = 5.9\%$ and 16.4% at the beginning and ending points of CTA, respectively (where l denotes the length of a single PPHCS).

In specimens S2 and S3, cracks occurred at $\delta = 4.1$ and 3.5 mm, respectively. The vertical load-displacement curve of S3 was similar to that of S1, but several sudden drops occurred in the CTA of S2. This is because a concentrated crack occurs at the middle joint of S2, resulting in premature fracture of the bottom bars of the connector due to strain concentration. However, $P_{CTA} = 16.72$ kN was greater than $P_{CAA} = 9.87$ kN in S2. In S3, the peak load increased to $P_{CTA} = 34.55$ kN, deformation capacity was improved, and no rebar was fractured. This result indicates that debonding of rebars can mitigate strain concentration effectively. In S2 and S3, δ/l was 4.6% and 5.2% at the beginning and 16.4% and 15.4% at the ending of CTA, respectively.

The ultimate displacement and load-carrying capacity of specimens S4 and S5 were significantly greater than those of the other specimens. In S4 and S5, cracks occurred at $\delta = 2.8$ and 7.0 mm, respectively. The CAA of S4 was not fully developed, and the vertical displacement corresponding to the development of CTA was larger than that of the other specimens. This is because the kinked reinforcement needs to be straightened gradually before generating the effective tension force, delaying the development of the load-carrying capacity in the early stage. Although effective ties were formed at the final stage, $P_{CTA} = 49.95$ kN in S4 was less than $P_{CTA} = 72.56$ kN in S5, indicating that the partial hinges greatly improved the deformation capacity without significant strength degradation. P_{CTA} of S5 was 64%, 334%, 110%, and 45% greater than that of S1–S4, respectively. δ/l was 6.9% and 25.3% at the beginning and ending of CTA in S4, and that for S5 was 5.3% and 24.3%, respectively.

At the same vertical displacement level, S1 exhibited the greatest load-carrying capacity due to CAA and CTA, and that of S4 was the lowest. This is because a higher tension force is developed in the connector bars of S1, and the tension force of connector bars in S4 cannot be fully developed at an early stage. The load-carrying capacities of S2, S3, and S5 using the same rebars are similar at the same vertical displacement level.

The relationships between the lateral displacement at the edge joint and the vertical displacement of the specimens are shown in Fig. 8. The peak values of horizontal reaction force and lateral displacement are shown in Table 3. For all specimens, outward lateral displacement (i.e., negative value) was observed first. As the vertical displacement increased, the outward lateral displacement was changed to inward lateral displacement gradually. In specimen S1, both the horizontal reaction force and lateral displacement in CAA were the largest, resulting in the greatest CAA among all specimens. On the other hand, the horizontal reaction force and lateral displacement of CAA in S2 were the lowest, developing the lowest CAA among all specimens except for specimen S4. In general, the load-carrying capacity of CAA is affected by the horizontal reaction force. However, in S4, regardless of the horizontal reaction force, the peak load of CAA was the lowest. This is because the kinked rebars need to be straightened first, and the tension force of the bottom bars at this stage cannot contribute to CAA.

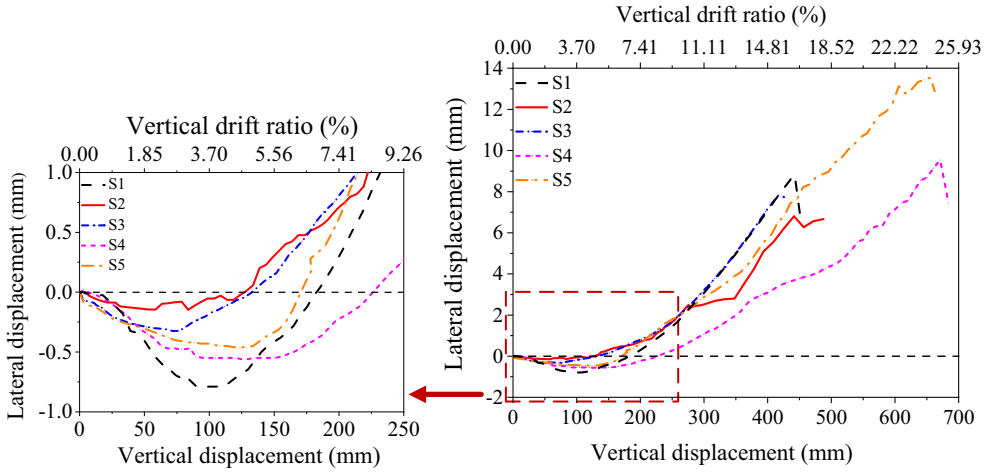

Fig. 8. Lateral displacement-vertical displacement relationships of test specimens.

Table 3. Peak horizontal reaction force and lateral displacement

Specimen	Peak horizontal reaction force		Peak lateral displacement	
	Compression (kN)	Tension (kN)	Outward (mm)	Inward (mm)
S1	17.97	175.85	0.73	8.86
S2	10.3	112.48	0.15	6.80
S3	12.76	140.02	0.33	7.82
S4	13.47	181.59	0.56	9.54
S5	12.66	241.41	0.46	13.61

The occurrence of transition points of all specimens was similar except S4, which was later than the other specimens. The horizontal reaction force in S4 was less than that of the other specimens at the same vertical displacement, resulting in the lowest lateral displacement and CTA at the same vertical displacement.

Failure Modes and Load Resistance Mechanisms

The failure modes of PPHCS specimens are illustrated in Fig. 9 and summarized in Table 4. Only one major crack was observed at the middle joint of specimens S1–S3, which appeared at the early stage and widened as the vertical displacement increased. However, more severe damage can be found in specimens S4 and S5. In S1, the middle joint gap opening increased to 36 mm, and a horizontal crack developed along the connectors [Fig. 9(b)]. Concrete crushing occurred at the top of the middle joint. Ultimately, concrete failed at the right joint, which resulted in the loss of effective ties. Although all inserted connectors remained intact, the load-carrying capacity decreased significantly. In S2, the middle joint gap opening increased to 45 mm, which resulted in the fracture of four bottom bars [Fig. 9(c)]. Concrete damage occurred at both edge joints, weakening the effectiveness of the left and right connectors. Compared to S1 and S2, except for the major crack at the middle joint, in which the gap opening was 35 mm, a smaller flexural crack developed at the end of the debonding area in S3 [Fig. 9(d)]. Ultimately, concrete was delaminated along the prestressing tendon at the right joint, significantly decreasing the load-carrying capacity. Due to the debonding of connector bars, the strain concentration was mitigated, and no rebar fracture occurred. In S4, two vertical cracks appeared at the left and right kinked bars of the middle joint, straightening the connectors, and the corresponding gap opening increased to 31 and 44 mm, respectively [Fig. 9(e)]. The connectors at the edge joints were also straightened, and concrete failed at the right joint. Ultimately, all straightened connectors effectively tied the two PPHCSs and provided progressive collapse resistance. In S5, the use of hinge detail at the middle joint significantly improved the deformation capacity, but concrete damage significantly occurred [Fig. 9(f)]. Effective ties were maintained to a certain extent at the end of the test.

The load resistance mechanism is shown in Fig. 9(a). As the vertical load increased, a crack occurred at the bottom of the middle joint. As the vertical displacement increased, the middle joint of the specimen moved downward gradually, resulting in the outward lateral displacement of the slabs. Thus, CAA due to the lateral constraints resisted the vertical load until the concrete crushed at the top of the middle joint. Thereafter, the vertical displacement increased further, and the compression force in concrete gradually transformed into tension in connectors. Similarly, due to the lateral constraints, CTA was developed. According to the failure mode of each specimen, the CTA of S1 and S3 significantly decreased due to serious damage to the right joint. In S2, CTA was contributed by only the top bars of the middle joint. On the other hand, in S4 and S5, CTA was effectively developed.

Slab Deflection

The distribution of the slab deflection (i.e., vertical displacement) of all specimens at failure is shown in Fig. 10. The slab deflection of S4 was the largest, followed by S5, and that of S1–S3 was similar. Although the specimen failure was concentrated on one side (i.e., the right side), the overall slab deflection was basically symmetric. As only concentrated loading was applied to the middle joint, single curvature deformation occurred. The slab rotation was less than the chord rotation [i.e., the ratio of the slab deflection to the slab span (DOD 2016)]. In the case of S4, the deflection of the slab showing brittle failure (right side) was larger than that of the other slab (left side), which also had an obvious deviation from the chord rotation, indicating that the left slab also reached a relatively large deflection at the end of the test. In S1–S3 and S5, basically symmetric deflection occurred at the middle joint, while the middle joint of S4 was tilted due to two significant cracks [refer to Fig. 9(e)].

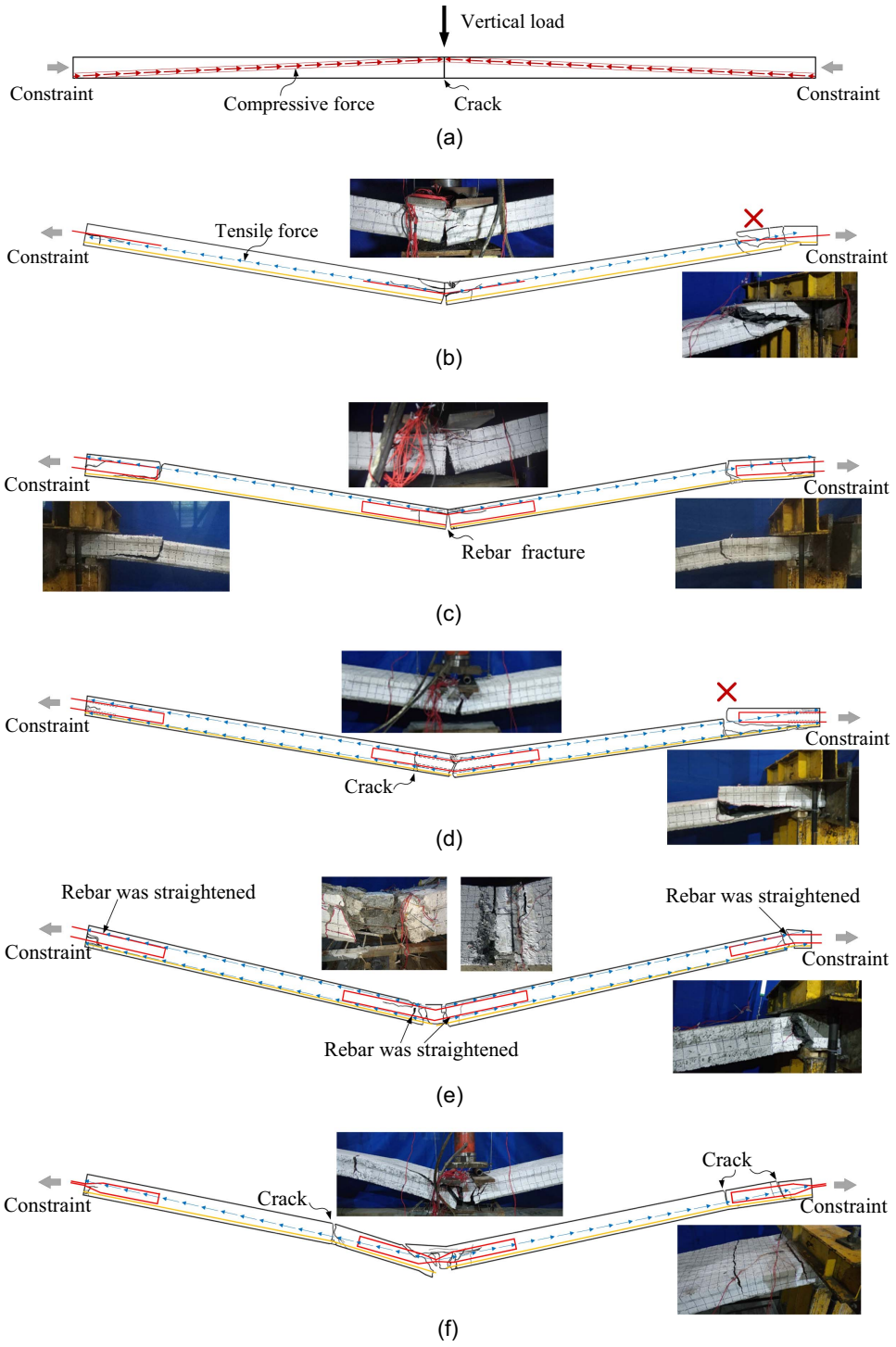

Fig. 9. Failure modes and load resistance mechanisms (unit: mm): (a) compressive arch action; (b) S1; (c) S2; (d) S3; (e) S4; and (f) S5.

Strain of Connector Reinforcement

The strain development of connector reinforcement in S1 is shown in Fig. 11(a). The reinforcement at section 2-2 (i.e., middle joint) yielded at $\delta = 25$ mm, and the strain gauge quickly malfunctioned. The strain development at section 2-2 was much faster than that at section 1-1 (i.e., left edge joint) because the vertical constraint at the edge joint directly resisted a part of the force transmitted from the middle joint. Thus, the tension force at the edge joint was less than that of the middle joint, and such a phenomenon was also found in the other specimens. The reinforcement strain at sections 4-4 and 5-5 was negligible, indicating that the embedment length of the connector reinforcement was reasonable to avoid bond failure. In S2, the bottom and top reinforcement at the middle joint yielded at $\delta = 5$ and 25 mm, respectively [Fig. 11(b)]. The top reinforcement at section 2-2 (i.e., 2-2T) was initially in compression and then changed to tension. Because the distance between the top reinforcement and slab surface was about 40 mm, the compression force in CAA was resisted by concrete only. The strain development of S3 was similar to that of S2 [Fig. 11(c)]. However, the

Table 4. Failure modes of test specimens

Specimen	Failure mode
S1	The width of the middle joint gap was 36 mm; a horizontal crack was developed along the connectors; concrete crushing occurred at the top of the middle joint; concrete failed at the right joint; and no rebar fracture occurred
S2	The width of the middle joint gap was 45 mm; fracture occurred at all bottom bars; and concrete damage occurred at both edge joints
S3	The width of the middle joint gap was 35 mm; a smaller flexural crack developed at the end of the debonding area; concrete delaminated along the prestressing tendon at the right joint; and no rebar fracture occurred
S4	Two vertical cracks appeared at the left (31 mm) and right (44 mm) kinked bars of the middle joint; concrete failed at the right joint; and no rebar fracture occurred
S5	An approximate hinge was generated in the middle joint; concrete at the middle joint was significantly damaged; concrete failed at the right joint; and no rebar fracture occurred

reinforcement at 2-2B and 2-2T yielded at $\delta = 26$ and 102 mm, respectively, which was significantly larger than that of S2. Further, the strain increase of S3 after yielding was slower than that of S2. This result indicates that the partial debonding detail effectively alleviates strain concentration. In S4, the large plastic strain of the reinforcement at 2-2B was maintained after the initial rapid development and then continued to increase rapidly [Fig. 11(d)]. This is because the kinked rebar needs to be straightened before it transfers the tension force completely. Although the top reinforcement was also straightened at the failure mode, the stress of the top reinforcement was still at a relatively low level, indicating that S4 would continue to resist the vertical load to some extent after concrete failure. In S5, the strain development at 2-2T and 2-2B was basically the same due to the use of a partial hinge [Fig. 11(e)]. The corresponding strain of S5 was less than that of S1 at the same displacement level, demonstrating better deformation capacity of the partial hinge connector. In summary, the ties of all specimens yielded, indicating that the ties played a key role in the large-deformation stage.

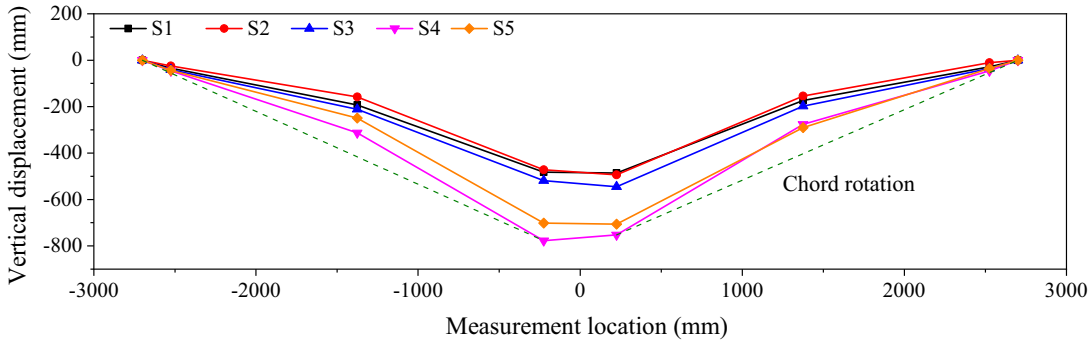

Fig. 10. Slab deflection at the end of the test.

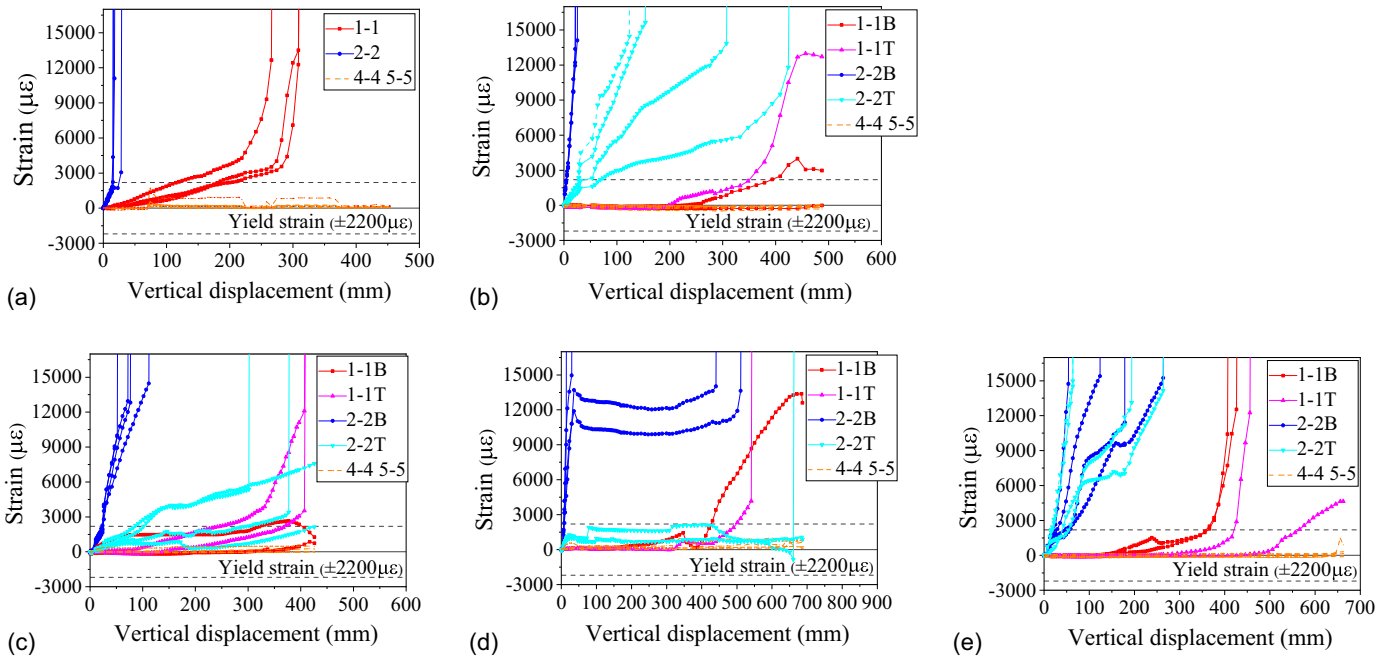

Fig. 11. Strain of connector reinforcement: (a) S1; (b) S2; (c) S3; (d) S4; and (e) S5.

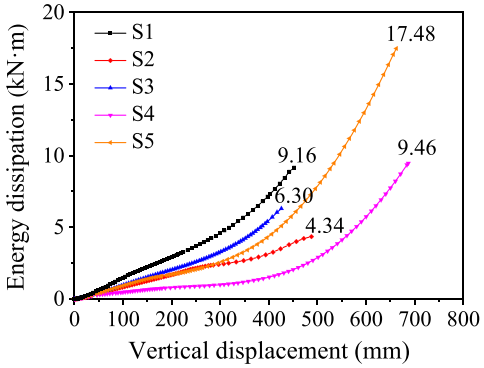

Fig. 12. Energy dissipation capacity of test specimens.

Energy Dissipation Capacity and Simplified Dynamic Assessment

Under progressive collapse, the vertical load applied to a substructure that losses supporting components exhibits a highly dynamic and nonlinear feature. Thus, when the progressive collapse resistance is evaluated, quasi-static study alone has some limitations. To supplement quasi-static test results, the energy dissipation capacity was evaluated, and a simplified dynamic assessment was conducted.

Energy Dissipation Capacity

In the energy balance principle, the work done by the applied gravity load is defined as an energy input. To resist progressive collapse, the strain energy generated in the substructure should be the same as the work generated by the gravity load. Thus, the energy dissipation capacity can be regarded as an effective index to evaluate the progressive collapse resistance of a structure. The strain energy (E) can be calculated as follows:

$$E = \int_0^{u_d} P_s(u)du \tag{1}$$

where u_d = ultimate displacement; and $P_s(u)$ = load-carrying capacity corresponding to $\delta = u$. It is noted that the strain energy of the specimens can be defined as the area under the vertical load-displacement curve.

The energy dissipation capacity of the PPHCS specimens in accordance with the vertical displacement is shown in Fig. 12. Specimen S5 exhibited the greatest energy dissipation capacity, which was 91%, 303%, 190%, and 85% greater than that of S1–S4, respectively. Specimen S2 exhibited the least energy dissipation capacity, which could hardly resist progressive collapse. As shown in Fig. 12, the increase rate of energy dissipation was affected by connection details, which can be considered the energy dissipation efficiency of the specimen approximately. Under the same level of vertical displacement, S1 and S4 dissipated the largest and least energy, respectively. This result indicates that the larger tension force of reinforcement dissipates the input energy more efficiently.

Simplified Dynamic Assessment

Based on the energy dissipation capacity of the PPHCS specimens, the dynamic resistance of the specimens can be simply evaluated. In general, the dynamic ultimate strength of a structure can be evaluated using a dynamic amplification factor (DIF). GSA (2003) utilizes a constant dynamic amplification factor (i.e., DIF = 2) for gravity loading above the damaged column. However, this load amplification is appropriate for a linear elastic response. Ruth et al. (2006) found that the upper bound of DIF for steel frames and RC moment frames were 1.5 and 1.4, respectively. Qian and Li (2012) reported that the DIF of RC moment frames was less than 1.38. Thus, the value of DIF is controversial at present, and the loading mechanism of RC moment frames would differ from that of PC slab cross-wall structures. Thus, to evaluate the dynamic resistance of PC slab cross-wall structures, a simplified dynamic assessment proposed by Izzuddin et al. (2008) was adopted in this study. This approach can convert the quasi-static response obtained by the quasi-static test into nonlinear dynamic behavior, which is called a pseudo-static response. The pseudo-static response (P_d) is determined from the cumulative strain energy divided by the corresponding displacement, and the accuracy of this method was verified by Tsai (2010). It is noted that in the simplified method, the energy dissipation caused by damping is not considered because the duration of progressive collapse is very short and the energy consumed by damping is relatively small

$$P_d = \frac{1}{u_d}E \tag{2}$$

The pseudo-static response of specimens S1–S5 is shown in Fig. 13. Table 5 compares the quasi-static response and pseudo-static response of S1–S5, and the DIF of all specimens is illustrated. Note that the DIF was simply defined as the ratio of the quasi-static response to the pseudo-static response in this study. As shown in Table 5, the pseudo-static response of S1–S3 decreased by approximately 50%, compared with the quasi-static response. For S4 and S5, the pseudo-static response decreased by more than 63%. The DIF ranges from 1.9 to 3.6 with a mean value of 2.5. This result indicates that the quasi-static response is much larger than the pseudo-static response, which would result in an unsafe design without considering dynamic characteristics.

The comparison of the pseudo-static response of specimens S1–S5 is shown in Fig. 14. Similar to the quasi-static response, S5 and S2 exhibited the greatest and least ultimate pseudo-static response, respectively. The ultimate quasi-static response of S4 was greater than that of S1 and S3. However, the ultimate pseudo-static response of S4 was less than that of S1 and S3. This is because although the CTA of S4 generates a greater peak load at a larger displacement than that of S1 and S3, insufficiently developed CAA of S4 decreases the area under the vertical load-displacement curve. It can be proved that dynamic loading has a significant effect on the evaluation of progressive collapse resistance.

Due to the hollow core of the slab section, the dead load (DL) of the slab is only 2.5 kN/m^2. According to GB 50009-2012 (SAC 2012), the live load (LL) is assumed to be 2 kN/m^2, and the volumetric weight of a brick wall is 18 kN/m^3. Based on the load combination of 1.2DL + 0.5LL according to DoD (2016), 13.64 kN was applied to the middle joint under normal serviceability (i.e., load line in Fig. 14). As shown in Fig. 14, the peak pseudo-static response of S2 was less than the load line, indicating that new energy balance could not be achieved and the structure was collapsed under this load level. On the other hand, the peak pseudo-static response of the other specimens was greater than the load line, indicating sufficient progressive collapse resistance. However, the pseudo-static response of S3–S5 satisfied the requirement of progressive collapse resistance at the CTA stage. In a word, without the full development of CTA, specimens S3–S5 would be collapsed, demonstrating the importance of CTA in progressive collapse resistance.

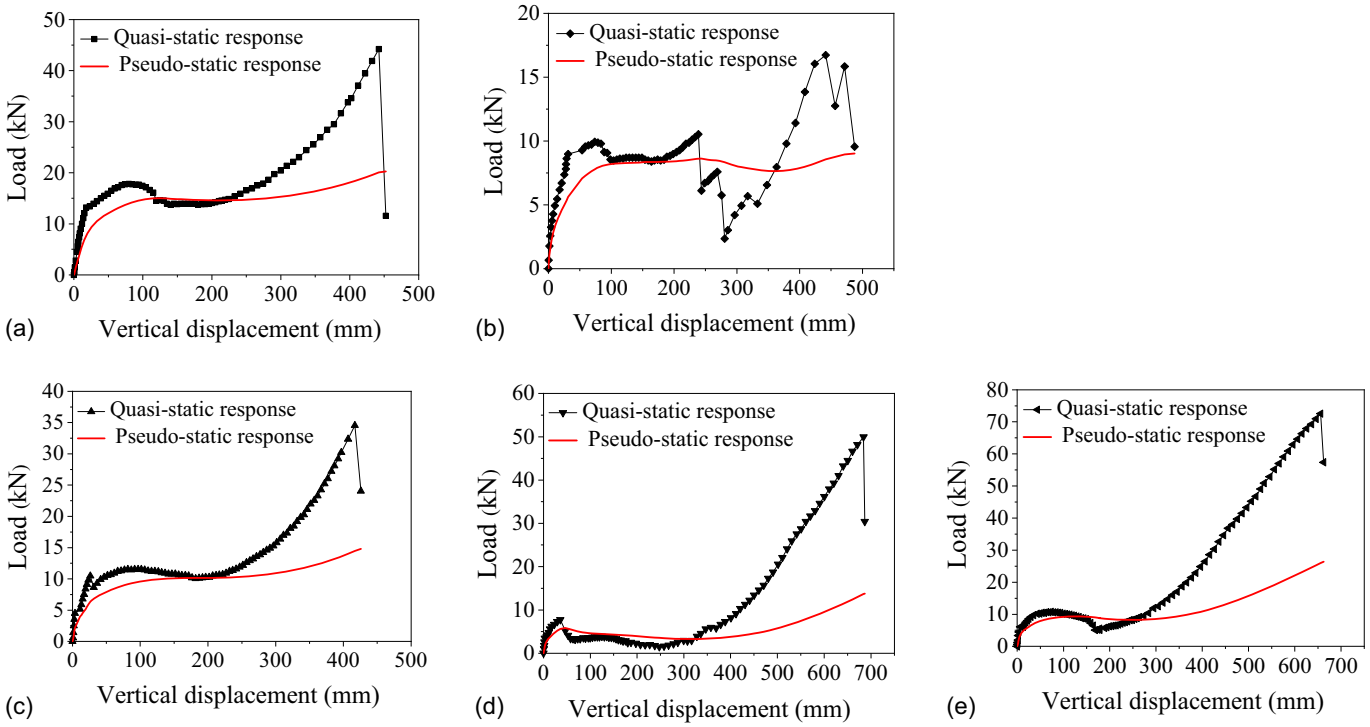

Fig. 13. Pseudo-static response of test specimens: (a) S1; (b) S2; (c) S3; (d) S4; and (e) S5.

Discussion and Future Work

In specimen S1, the load-carrying capacity significantly decreased by L1 due to concrete failure at the slab end under a negative moment, and the remaining capacity (L2) was developed by the reinforcement ties (Fig. 15). For S1, the ratio of L2/(L1 + L2) was only 26%, while that of S2–S5 was around 60%, indicating that once concrete cracking occurred, the load-carrying capacity of S1 was lost almost completely. This is because the stiffness of S1 is enhanced by using larger reinforcement of the connector, resulting in severe brittle failure. Thus, to avoid significant brittle damage in practice, it is not recommended to obtain higher load-carrying capacity by simply increasing the diameter of the connector reinforcement.

Although effective ties were generated in S4 at the final stage, the load-carrying capacity of S4 was the weakest at the early stage. Thus, an improved connector can be designed by combining the characteristics of the used connectors. For example, an additional reinforcement and/or partial debonding detail can be used in the middle of the connector in S4. However, further studies are needed to investigate the structural performance of the improved connector in the progressive collapse resistance of PPHCSs.

Table 5. Comparison of quasi-static response and pseudo-static response

Specimen	Quasi-static response (kN)	Pseudo-static response (kN)	Decrease ratio (%)	DIF
S1	44.24	20.25	54.2	2.2
S2	16.72	9.01	46.1	1.9
S3	34.55	14.80	57.2	2.3
S4	49.95	13.78	72.4	3.6
S5	72.56	26.39	63.6	2.7

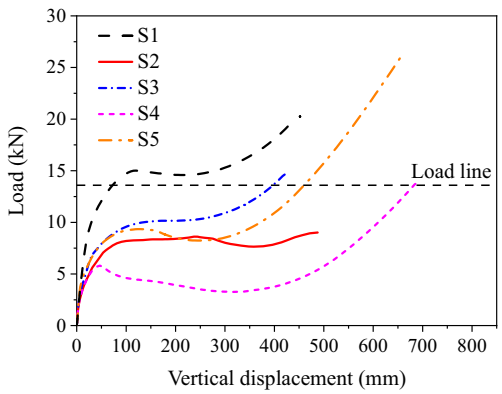

Fig. 14. Comparison of pseudo-static responses.

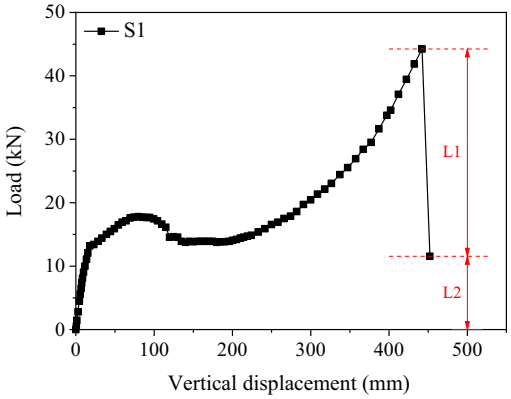

Fig. 15. Load-carrying capacity at the failure point.

Based on the full incremental dynamic assessment and direct comparison with a quasi-static response, an in-depth evaluation of DIF is another potential development, potentially greatly simplifying the analysis of the dynamic performance of similar structures.

Conclusions

In the present study, five types of connectors and corresponding specimens were designed, and the progressive collapse resistance was investigated by a quasi-static test. The structural performance according to the load resistance mechanism was evaluated. Based on energy dissipation capacity, the pseudo-static response of the specimens was estimated using a simplified dynamic assessment to further evaluate the progressive collapse resistance. The principal findings can be drawn as follows:

1. The test results showed that the peak load of CTA was greater than that of CAA, indicating that effective ties were generated between slabs. In CAA, the horizontal reaction force was in compression. As the vertical displacement increased, the horizontal reaction force transferred to tension in the CTA stage. The ultimate displacement and load-carrying capacity of specimens S4 and S5 were significantly greater than those of the other specimens, showing the effectiveness of kinked rebar and partial hinge details. The ultimate strength (72.56 kN) of S5 using partial hinge was 64%, 334%, 110%, and 45% greater than that of S1–S4, respectively.
2. Failure modes showed that only one major crack was observed in the middle joint of specimens S1–S3. However, more severe damage was found in specimens S4 and S5. In S2, premature fracture occurred at the bottom reinforcement of the connector due to strain concentration. S4 and S5 effectively maintained CTA at the end of the test.
3. The rebar strain at the middle joint was much more quickly developed than that of the edge joint. Partial debonding detail alleviated strain concentration effectively. In S4, the large plastic strain of the bottom kinked bars at the middle joint was maintained, showing a considerable safety reserve. The use of a partial hinge in S5 delayed the strain development of the connector reinforcement at the middle joint, improving the deformation capacity.
4. To evaluate the progressive collapse resistance more reasonably, the energy dissipation capacity and simplified dynamic assessment were investigated. The energy dissipation capacity of S5 was 91%, 303%, 190%, and 85% greater than that of S1–S4, respectively. Similar to the quasi-static response, S5 and S2 exhibited the greatest and least ultimate pseudo-static response, respectively. Unlike the quasi-static response, the ultimate pseudo-static response of S4 was worse than that of S1 and S3. This result indicates that the dynamic feature of the load has a significant effect on the evaluation of structural resistance against progressive collapse.

Data Availability Statement

Some or all data, models, or code generated or used during the study are available from the corresponding author upon request.

Acknowledgments

The authors sincerely appreciate the funding support provided by the National Natural Science Foundation of China (NSFC) (No. 51878264), the National Key Research and Development Program of China (Nos. 2016YFC0701400 and 2016YFC0701308), the Key Research and Development Program of Changsha City (kq1801010), the Key Research and Development Program of Hunan province (2022SK2096), the National Research Foundation of Korea (NRF) Grant funded by the Korea Government (MSIT) (No. 2021R1A4A3030117), and the Korea Agency for Infrastructure Technology Advancement (KAIA) funded by the Ministry of Land, Infrastructure and Transport (Grant 22RMPP-C163162-02).

References

Adam, J. M., F. Parisi, J. Sagaseta, and X. Lu. 2018. "Research and practice on progressive collapse and robustness of building structures in the 21st century." *Eng. Struct.* 173 (Oct): 122–149. https://doi.org/10.1016/j.engstruct.2018.06.082.

Aguado, J. V., V. Albero, A. Espinos, A. Hospitaler, and M. L. Romero. 2016. "A 3D finite element model for predicting the fire behavior of hollow-core slabs." *Eng. Struct.* 108 (Feb): 12–27. https://doi.org/10.1016/j.engstruct.2015.11.008.

Alogla, K., L. Weekes, and L. Augusthus-Nelson. 2016. "A new mitigation scheme to resist progressive collapse of RC structures." *Constr. Build. Mater.* 125 (Oct): 533–545. https://doi.org/10.1016/j.conbuildmat.2016.08.084.

Alshaikh, I. M. H., A. A. Abadel, and M. Alrubaidi. 2022. "Precast RC structures' progressive collapse resistance: Current knowledge and future requirements." *Structures* 37 (Mar): 338–352. https://doi.org/10.1016/j.istruc.2021.12.086.

Alshaikh, I. M. H., B. H. A. Bakar, E. A. H. Alwesabi, and H. M. Akil. 2020. "Experimental investigation of the progressive collapse of reinforced concrete structures: An overview." *Structures* 25 (Jun): 881–900. https://doi.org/10.1016/j.istruc.2020.03.018.

ASCE. 2005. *Minimum design loads for buildings and other structures*. Reston, VA: ASCE.

Baran, E. 2015. "Effects of cast-in-place concrete topping on flexural response of precast concrete hollow-core slabs." *Eng. Struct.* 98 (Sep): 109–117. https://doi.org/10.1016/j.engstruct.2015.04.017.

Brunesi, E., and R. Nascimbene. 2015. "Numerical web-shear strength assessment of precast prestressed hollow core slab units." *Eng. Struct.* 102 (Nov): 13–30. https://doi.org/10.1016/j.engstruct.2015.08.013.

Corley, W. G., P. F. Mlakar Sr., M. A. Sozen, and C. H. Thornton. 1998. "The Oklahoma City bombing: Summary and recommendations for multihazard mitigation." *J. Perform. Constr. Facil.* 12 (3): 100–112. https://doi.org/10.1061/(ASCE)0887-3828(1998)12:3(100).

Cuenca, E., and P. Serna. 2013. "Failure modes and shear design of prestressed hollow core slabs made of fiber-reinforced concrete." *Composites, Part B* 45 (1): 952–964. https://doi.org/10.1016/j.compositesb.2012.06.005.

DOD (Department of Defense). 2016. *Design of buildings to resist progressive collapse*. Washington, DC: DOD.

Elsanadedy, H. M., T. H. Almusallam, Y. A. Al-Salloum, and H. Abbas. 2017. "Investigation of precast RC beam-column assemblies under column-loss scenario." *Constr. Build. Mater.* 142 (Jul): 552–571. https://doi.org/10.1016/j.conbuildmat.2017.03.120.

Feng, P., H. Qiang, W. Qin, and M. Gao. 2017. "A novel kinked rebar configuration for simultaneously improving the seismic performance and progressive collapse resistance of RC frame structures." *Eng. Struct.* 147 (Sep): 752–767. https://doi.org/10.1016/j.engstruct.2017.06.042.

Griffiths, H., A. Pugsley, and O. A. Saunders. 1968. *Report of the inquiry into the collapse of flats at Ronan Point, Canning Town: Presented to the Minister of Housing and Local Government*. London: His Majesty's Stationery Office.

GSA (General Services Administration). 2003. *Progressive collapse analysis and design guidelines for new federal office buildings and major modernization projects*. Washington, DC: GSA.

Izzuddin, B. A., A. G. Vlassis, A. Y. Elghazouli, and D. A. Nethercot. 2008. "Progressive collapse of multi-storey buildings due to sudden column loss—Part I: Simplified assessment framework." *Eng. Struct.* 30 (5): 1308–1318. https://doi.org/10.1016/j.engstruct.2007.07.011.

Kakhki, S. A. E., A. Kheyroddin, and A. Mortezaei. 2022. "Evaluation of the progressive collapse of the reinforced concrete frames considering

the soil–structure interaction: Parametric study based on the sensitivity index." *Int. J. Concr. Struct. Mater.* 16 (1): 38. https://doi.org/10.1186/s40069-022-00523-x.

Kankeri, P., and S. S. Prakash. 2016. "Experimental evaluation of bonded overlay and NSM GFRP bar strengthening on flexural behavior of precast prestressed hollow core slabs." *Eng. Struct.* 120 (Aug): 49–57. https://doi.org/10.1016/j.engstruct.2016.04.033.

Kankeri, P., and S. S. Prakash. 2017. "Efficient hybrid strengthening for precast hollow core slabs at low and high shear span to depth ratios." *Compos. Struct.* 170 (Jun): 202–214. https://doi.org/10.1016/j.compstruct.2017.03.034.

Mansour, F. R., S. A. Bakar, I. S. Ibrahim, A. K. Marsono, and B. Marabi. 2015. "Flexural performance of a precast concrete slab with steel fiber concrete topping." *Constr. Build. Mater.* 75 (Jan): 112–120. https://doi.org/10.1016/j.conbuildmat.2014.09.112.

Michelini, E., P. Bernardi, R. Cerioni, and B. Belletti. 2020. "Experimental and numerical assessment of flexural and shear behavior of precast prestressed deep hollow-core slabs." *Int. J. Concr. Struct. Mater.* 14 (1): 1–17. https://doi.org/10.1186/s40069-020-00407-y.

PCA (Portland Cement Association). 1975. *Design and construction of large-panel concrete structures*. Rep. 1 to 6, and Supplement Rep. of A, B, C. US Dept. of Housing and Development. Skokie, IL: PCA.

Qian, K., and B. Li. 2012. "Dynamic performance of RC beam-column substructures under the scenario of the loss of a corner column—Experimental results." *Eng. Struct.* 42 (Sep): 154–167. https://doi.org/10.1016/j.engstruct.2012.04.016.

Qian, K., and B. Li. 2013. "Strengthening and retrofitting of RC flat slabs to mitigate progressive collapse by externally bonded CFRP laminates." *J. Compos. Constr.* 17 (4): 554–565. https://doi.org/10.1061/(ASCE)CC.1943-5614.0000352.

Qian, K., and B. Li. 2018. "Performance of precast concrete substructures with dry connections to resist progressive collapse." *J. Perform. Constr. Facil.* 32 (2): 04018005. https://doi.org/10.1061/(ASCE)CF.1943-5509.0001147.

Qiang, H., J. Yang, P. Feng, and W. Qin. 2020. "Kinked rebar configurations for improving the progressive collapse behaviours of RC frames under middle column removal scenarios." *Eng. Struct.* 211 (May): 110425. https://doi.org/10.1016/j.engstruct.2020.110425.

Ravasini, S., B. Belletti, E. Brunesi, R. Nascimbene, and F. Parisi. 2021. "Nonlinear dynamic response of a precast concrete building to sudden column removal." *Appl. Sci.* 11 (2): 599. https://doi.org/10.3390/app11020599.

Ruth, P., K. A. Marchand, and E. B. Williamson. 2006. "Static equivalency in progressive collapse alternate path analysis: Reducing conservatism while retaining structural integrity." *J. Perform. Constr. Facil.* 20 (4): 349–364. https://doi.org/10.1061/(ASCE)0887-3828(2006)20:4(349).

SAC (Standardization Administration of China). 2010. *Code for design of concrete structures*. GB 50010-2010. Beijing: China Architecture & Building Press.

SAC (Standardization Administration of China). 2012. *Load code for the design of building structures*. GB 50009-2012. Beijing: China Architecture & Building Press.

Sarkis, A. I., F. Büker, T. J. Sullivan, K. J. Elwood, E. Brunesi, and L. S. Hogan. 2022. "Aspects affecting the nonlinear behavior of precast prestressed hollow-core units failing in shear." *Struct. Concr.* 23 (5): 3021–3038. https://doi.org/10.1002/suco.202100579.

Seffen, K. A. 2008. "Progressive collapse of the world trade center: Simple analysis." *J. Eng. Mech.* 134 (2): 125–132. https://doi.org/10.1061/(ASCE)0733-9399(2008)134:2(125).

Stinger, S. M., and S. L. Orton. 2013. "Experimental evaluation of disproportionate collapse resistance in reinforced concrete frames." *ACI Struct. J.* 110 (3): 521–529. https://doi.org/10.14359/51685609.

Tohidi, M., and C. Baniotopoulos. 2017. "Effect of floor joint design on catenary actions of precast floor slab system." *Eng. Struct.* 152 (Dec): 274–288. https://doi.org/10.1016/j.engstruct.2017.09.017.

Tohidi, M., and A. Janby. 2020. "Finite-element modeling of progressive failure for floor-to-floor assembly in the precast cross-wall structures." *J. Struct. Eng.* 146 (6): 04020087. https://doi.org/10.1061/(ASCE)ST.1943-541X.0002588.

Tohidi, M., J. Yang, and C. Baniotopoulos. 2014. "Numerical evaluations of codified design methods for progressive collapse resistance of precast concrete cross wall structures." *Eng. Struct.* 76 (Oct): 177–186. https://doi.org/10.1016/j.engstruct.2014.06.034.

Tsai, M. H. 2010. "An analytical methodology for the dynamic amplification factor in progressive collapse evaluation of building structures." *Mech. Res. Commun.* 37 (1): 61–66. https://doi.org/10.1016/j.mechrescom.2009.11.001.

Venanzi, I., M. Breccolotti, A. D'Alessandro, and A. L. Materazzi. 2014. "Fire performance assessment of HPLWC hollow core slabs through full-scale furnace testing." *Fire Saf. J.* 69 (Oct): 12–22. https://doi.org/10.1016/j.firesaf.2014.07.004.

Yang, X. J., F. Lin, and X. L. Gu. 2021. "Experimental study on a novel method to improve progressive collapse resistance of RC frames using locally debonded rebars." *J. Build. Eng.* 41 (Sep): 102428. https://doi.org/10.1016/j.jobe.2021.102428.

Yi, W. J., Q. F. He, Y. Xiao, and S. K. Kunnath. 2008. "Experimental study on progressive collapse-resistant behavior of reinforced concrete frame structures." *ACI Struct. J.* 105 (4): 433. https://doi.org/10.14359/19857.

Yi, W. J., F. Yi, and Y. Zhou. 2021. "Experimental studies on progressive collapse behavior of RC frame structures: Advances and future needs." *Int. J. Concr. Struct. Mater.* 15 (1): 31. https://doi.org/10.1186/s40069-021-00469-6.

Yu, J., and K. H. Tan. 2014. "Special detailing techniques to improve structural resistance against progressive collapse." *J. Struct. Eng.* 140 (3): 04013077. https://doi.org/10.1061/(ASCE)ST.1943-541X.0000886.